

Discovery of a Strongly Lensed Galaxy at $z = 3.9$ behind a $z = 0.83$ Galaxy Cluster *

Keiichi UMETSU ¹, Masayuki TANAKA ², Tadayuki KODAMA ^{3,5},

Ichi TANAKA ⁴, Toshifumi FUTAMASE ⁴, Nobunari KASHIKAWA ³, Takako HOSHI ^{3,6}

¹*Institute of Astronomy and Astrophysics, Academia Sinica, P.O. Box 23-141, Taipei 106, Taiwan, Republic of China*
keiichi@asiaa.sinica.edu.tw

²*Department of Astronomy, School of Science, University of Tokyo, Tokyo 113-0033*

³*National Astronomical Observatory of Japan, Mitaka, Tokyo 181-8588, Japan*

⁴*Astronomical Institute, Tohoku University, Aoba-ku, Sendai 980-8578*

⁵*European Southern Observatory, Karl-Schwarzschild-Str. 2, D-85748, Garching, Germany*

⁶*Department of Physics, Meisei University, 2-1-1 Hodokubo, Hino, Tokyo 191-8605, Japan*

(Received ; accepted)

Abstract

We report the discovery and spectroscopic confirmation of three gravitationally-lensed images of a galaxy at $z = 3.9$ in the background of a distant, rich cluster of galaxies at $z = 0.83$, on the basis of observations with Faint Object Camera And Spectrograph (FOCAS) on the Subaru telescope. We construct a simple lens model of the cluster mass distribution based on Jee et al.'s weak lensing mass estimates from deep, high-resolution images by Advanced Camera for Surveys (ACS) on the Hubble Space Telescope. The lens model can account simultaneously for the observed image configuration and the flux ratio of the closer pair located close to the critical curve. The parities of the three images are also consistent with the lensing hypothesis. Since this galaxy is apparently bright ($i'_{AB} \sim 23.7$) for its redshift due to the magnification, it serves as a good high redshift target on which we can make extensive and detailed studies based on multi-wavelength imaging and spectroscopy.

Key words: cosmology: gravitational lensing — galaxies: clusters: individual (RX J0152.7–1357) —

1. Introduction

Strong gravitational lensing due to the dense cores of clusters of galaxies leads to the formation of multiple images and giant luminous arcs of background galaxies. The lensing observables such as image positions and flux-ratios in turn provide strong constraints on the underlying gravitational potential of the lensing clusters. The strongly lensed images of background galaxies have therefore been powerful observational tools to probe the mass distribution in cluster cores (Mellier et al. 1993; Kneib et al. 1993, 1996, 2003; Hattori, Makino, & Kneib 1999; Molikawa & Hattori 1999; Broadhurst et al. 2005).

Exploring high- z galaxies is extremely important for understanding unsolved physical properties of forming galaxies as well as understanding the cosmic reionization history. The bottleneck is that such high- z forming galaxies are too faint to be observed with present-day telescopes due to the $(1+z)^4$ -dependence of the surface-brightness dimming effect. The most promising method is to utilize the gravitational magnification by clusters as a biggest natural telescope – Gravitational Lens Telescope (Ellis et al. 2001; Hu et al. 2002; Kneib et al. 2004). Furthermore, detailed study of high redshift galaxies can only be made for strongly lensed hence magnified galaxies (e.g., Pettini

et al. 2002 on cB58).

We have discovered a high- z lensed galaxy during the course of spectroscopic follow-up of the RXJ0152.7–1357 cluster at $z = 0.83$ as a part of our distant cluster project on the Subaru called PISCES (Kodama et al. 2005). In this paper, we present the spectroscopic and photometric properties of the newly discovered triple lensed images based on the observational data taken with the ground-based Subaru telescope as well as on the data with the high-resolution archival Advanced Camera for Surveys (ACS) on the Hubble Space Telescope (HST). A gravitational lens model of the cluster mass distribution is developed for the three lensed images. Throughout the paper we assume a Λ -dominated flat cosmology with $\Omega_m = 0.27, \Omega_\Lambda = 0.73$, and $h = 0.7$, and we use magnitudes given in the AB system.

2. Identification of the Lensed Objects

The lensed objects were first found as those having very similar colors in $VRi'z'$ based on the optical imaging with Suprime-Cam on the Subaru telescope (see Kodama et al. 2005 for details of the optical data). The photometric properties of the objects are summarized in Table 1. All the three objects show strong continuum breaks in the $V - R$ color (~ 0.9) with a relatively flat SED at longer wavelength regime. These photometric properties suggest that their redshifts are high ($z \sim 4$) in analogy to Lyman

* Based in part on data collected at the Subaru Telescope, which is operated by the National Astronomical Observatory of Japan.

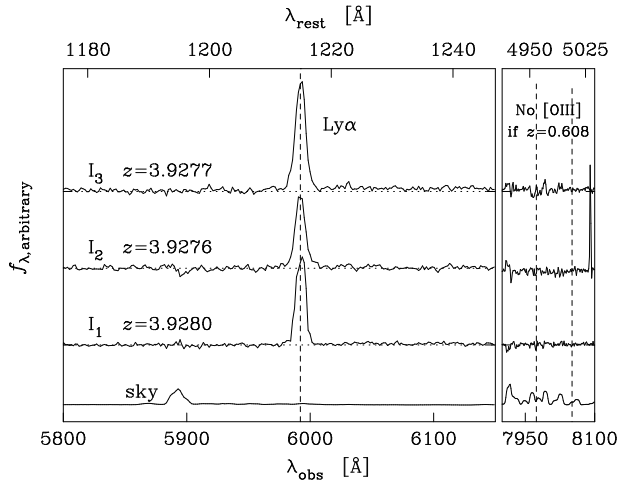


Fig. 1. The optical spectra of three multiple images (I_1, I_2, I_3) obtained with FOCAS on the Subaru telescope. The zero-flux levels are indicated with horizontal dotted lines.

break galaxies.

We have conducted spectroscopic follow-up observations during 11–14 October 2004 with FOCAS (Kashikawa et al. 2002) in the MOS mode. We used a 300 lines mm^{-1} grating blazed at 5500 \AA with the order-cut filter SY47. The wavelength coverage was between 4700 \AA and 9400 \AA with a pixel resolution of $1.40 \text{ \AA pixel}^{-1}$. A slit width was set to $0''.8$, which gave a resolution of $\lambda/\Delta\lambda \sim 500$. We obtained four 1800s exposures for each object nodded by $\sim 0''.6$ for each shot. The object I_2 was slipped out of the slit for one shot due to the nodding, and the net exposure on this object is $3 \times 1800\text{s}$. Data reduction was performed in a standard manner using *IRAF*. The objects I_1 and I_2 were very close to the spatial edge of the slits, and hence we will not discuss relative fluxes of these objects from the spectra. Figure 1 shows the obtained spectra of the the three images under concern. All the three show a strong emission line around $\lambda_{\text{obs}} = 5992 \text{ \AA}$. The emission line profile for each object was fitted with a Gaussian. The central wavelengths of the lines are 5992.41 \AA , 5991.95 \AA , and 5992.11 \AA for I_1 , I_2 , and I_3 , respectively, with a statistical error of $\sim 0.3 \text{ \AA}$. Therefore, the objects lie at the same redshift within the errors. The objects I_1 and I_3 show a clear continuum break shortward of this line, although no such break is seen in I_2 due to the low S/N . No other lines are observed in the spectra. These objects are either (1) a gravitationally lensed $\text{Ly}\alpha$ emitter at $z = 3.928$ or (2) foreground [OII] emitters at $z = 0.608$. The latter possibility is rejected, however. We observe no [OIII] lines at the expected wavelength as shown in Fig. 1. It is highly unlikely that galaxies show such a strong [OII] emission without any detectable [OIII] emission. The photometric properties of the objects are inconsistent with a $z = 0.608$ galaxy either. Their $V - R$ and $R - i'$ colors are too red for their $i' - z'$ colors to be star forming galaxies at $z \sim 0.6$. We therefore conclude that these objects are $\text{Ly}\alpha$ emitters at $z = 3.928$. Note that the rms error in the redshifts is $\sigma(z) \sim 3 \times 10^{-4}$. In summary, these objects show very similar photometric properties and they lie at

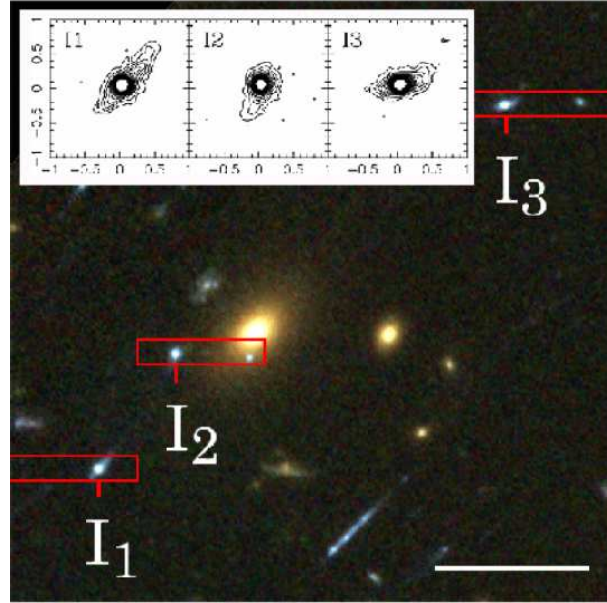


Fig. 2. Zoom-in view of a $20'' \times 20''$ region around the three gravitationally-lensed objects (I_1, I_2, I_3) in the HST/ACS composite color image constructed using F675W, F775W, and F850LP filters. The stick at the bottom right has a $5''$ length. The red open rectangles indicate the slit locations for the Subaru/FOCAS multi object spectroscopy of (I_1, I_2, I_3). The inset plots show the surface brightness contours of (I_1, I_2, I_3) from the F675W-band data. The coordinates are in arcseconds. The lowest contour and the contour interval are both at a 3σ rms noise level of $25.06 \text{ mag arcsec}^{-2}$.

exactly the same redshift – these facts strongly suggest that they are originally a single galaxy strongly lensed by the foreground cluster at $z = 0.83$.

We also obtained the “on-the-fly” processed HST/ACS images of the field from the HST archive (HST GTO Proposal 9290: Ford, H.). The cluster was observed in a 2×2 mosaic pattern with an overlap of $\sim 50''$ regions in F675W, F775W, and F850LP filters. The total exposure per pointing is about 4.8 ks for each filter. We show in Fig. 2 the HST image of the lensed objects and the Subaru image in Fig. 3. The objects all apparently look like the edge-on disk, which is probably due to the effect of strong lensing.

3. Strong Gravitational Lensing

3.1. Lens Model

The RXJ0152 gravitational lens system shows the collinear, three multiple images (I_1, I_2, I_3) of a source galaxy at $z = 3.9$, from which one expects that the lensed images could be associated with a cusp caustic produced by an elliptical potential (e.g., Schneider, Ehlers, & Falco 1992). In constructing a lens model of the cluster mass distribution, we closely follow weak lensing mass estimates by Jee et al. (2005) based on the HST/ACS observations with superb angular-resolution and photometric-depth. We adopt Jee et al.’s parameterized singular isothermal ellipsoid model (SIE: Kormann et al. 1994; King & Schneider

Table 1. Photometric properties of three gravitationally lensed images from Subaru/Suprime-Cam and HST/ACS data*

Object	R.A. (J2000)	Dec. (J2000)	i'^{\dagger} (AB-mag)	$V - R$ (AB-mag)	$R - i'$ (AB-mag)	$i' - z'$ (AB-mag)	r_h^{\ddagger} ($''$)
I_1	01 52 45.32	-13 57 08.6	23.70 ± 0.04	$+0.85 \pm 0.01$	-0.03 ± 0.01	-0.07 ± 0.03	0.141
I_2	01 52 45.14	-13 57 04.9	24.05 ± 0.04	$+0.90 \pm 0.02$	$+0.08 \pm 0.02$	$+0.18 \pm 0.03$	0.125
I_3	01 52 44.41	-13 56 56.7	23.89 ± 0.04	$+0.88 \pm 0.01$	-0.06 ± 0.02	$+0.02 \pm 0.03$	0.127

* The total magnitudes 'MAG_AUTO' (SExtractor) are used for i'_{AB} . Photometric apertures of $1''$ are used for color measurements.

‡ Half-light radii (FLUX_RADIUS by SExtractor) measured in the HST/ACS F675W-band image

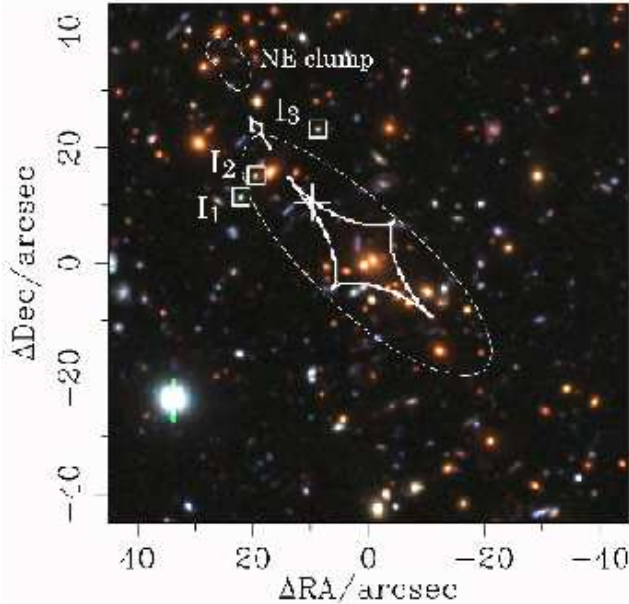


Fig. 3. Vri' color image of the central $90'' \times 90''$ region of RXJ0152 ($z = 0.83$) obtained with Subaru/Suprime-Cam. North is top and East is left. Also overlaid are the caustic (thick solid lines) and the critical curves (thin dashed lines) predicted by our best fitting model. The cross represents the predicted position of the source galaxy at $z = 3.9$. The open squares represent the predicted positions of the multiple images (I_1, I_2, I_3).

2001) centered between the two central brightest cluster galaxies, for describing the elongated global mass distribution. The SIE requires three model parameters: Einstein radius θ_E , minor-to-major axis ratio $f (= b/a)$, and orientation angle α . Jee et al. obtained the best-fit parameters of $\theta_E = 7''.19 \pm 0''.72$ ($z_s = 1.3$) and $f = 0.36 \pm 0.1$. This Einstein angle corresponds to the 1-D velocity dispersion of $\sigma_v^{\text{SIE}} = 940 \pm 168 \text{ km s}^{-1}$. For the source redshift of $z_s = 3.9$, this angle is scaled to $\theta_E = 15''.4$. The cluster contains several mass clumps associated with the cluster galaxy concentrations. As the three images are located in between the cluster center and the North-East substructure (mass clump B of Jee et al.), we take this clump into account in our lens model in the following way: We assume the clump mass of $M = 3.4 \times 10^{13} M_\odot$ estimated by Jee et al. is the virial mass of the clump. We then convert the mass into the 1-D velocity dispersion of an SIS halo ($\sigma_v^{\text{SIS}} \propto M^{1/3}$: see Bartelmann, King, & Schneider

2001). Accordingly, our model consists of one SIE as the global cluster halo and one SIS as the North-East substructure. We treat the SIE parameters (θ_E, f, α) and the (un-lensed) source position θ_S as free parameters of our lens model.

We then constrain the 5 model parameters via χ^2 -fitting to the observation data: the positions and the fluxes of the three images. In the model-fitting, we use as constraints the three image positions θ_{I_k} ($k = 1, 2, 3$) relative to the center of the SIE halo; we further include the flux ratio I_2/I_1 of the closer pair as it gives a strong constraint on the location of the critical curve. The χ^2 is then given as

$$\chi^2 = \sum_{k=1}^3 \frac{(\theta_{I_k} - \theta_{I_k}^M)^2}{\sigma_{\text{pos}}^2} + \frac{[(I_2/I_1) - (I_2/I_1)^M]^2}{\sigma_{I_2/I_1}^2}, \quad (1)$$

where quantities with superscript M denote the model predictions, σ_{pos} is the positional uncertainty of the multiple images, $\sigma_{\text{pos}} \approx 0''.1$, and σ_{I_2/I_1} is the rms error of the flux ratio I_2/I_1 . The image positions θ_I of a source with the position θ_S are obtained by solving the lens equation $\theta_S = \theta_I - \nabla\psi(\theta_I)$ (Schneider et al. 1992) with the effective lensing potential $\psi = \psi_{\text{SIE}} + \psi_{\text{SIS}}$ in sum of an SIE and an SIS potential.

3.2. Model Predictions v.s. Observations

We show in Fig. 3 the derived best-fit model of the RXJ0152 lens system overlaid on the Subaru image. The minimum χ^2 is $\chi_{\text{min}}^2/\text{dof} = 2.03/2$ for 2 degrees of freedom (dof). We quote the best-fit SIE parameters are $\theta_E = 14''.3_{-0.3}^{+0.4(+1.1)}$, $f = 0.25_{-0.03(-0.07)}^{+0.03(+0.08)}$, and $\alpha = 47.^\circ 7 \pm 0.2(\pm 0.4)$ measured East of North, with the 1σ (2σ) errors estimated from $\Delta\chi^2 \equiv \chi^2 - \chi_{\text{min}}^2 = 1$ (4) in the 5 parameter space.

The predicted source position is inside and close to a cusp caustic produced by the main cluster potential as expected. For such an image configuration, the image I_2 is predicted to have opposite parity as I_1 and I_3 . In particular, the closest images (I_1, I_2) are mirror images of each other with respect to the critical curve (see Fig. 3). The high-resolution ACS images reveal more detailed structures of the lensed images that were not spatially resolved in the Subaru images. Figure 2 clearly shows that the observed image parities are consistent with the lensing hypothesis: each image contains a bright core and extended emission with lower surface brightness, and a clear mirror symmetry between I_1 and I_2 is seen in the HST/ACS data. The predicted amplifications using the best-fit model are

$\mu_1 = 7.2$, $\mu_2 = 5.8$, and $\mu_3 = 3.0$ for I_1, I_2 , and I_3 , respectively. The total amplification factor over the three images is hence ≈ 16 . Accordingly, the predicted magnification ratios are $I_2/I_1 = 0.80$ and $I_3/I_1 = 0.42$, whereas the flux ratios from the Subaru i' -band data are $I_2/I_1 = 0.82 \pm 0.04$ and $I_3/I_1 = 0.89 \pm 0.05$. Our simple lens model thus reproduces correctly the observed flux ratio of I_2/I_1 while it fails for I_3/I_1 ; more than a factor 2 smaller than the observed flux ratio. In this study, we will not assess the significance of the difference between the observed and predicted flux-ratios for I_3/I_1 as it requires more detailed lens modeling for constraining all possible substructures (cf. Kneib et al. 1996). It is expected that the image I_3 could be easily magnified by local perturbers since its angular size (see Table 1) is sufficiently small compared with that of the lensing potential of possible perturbers (Chiba 2002).

4. Intrinsic Properties of the Source Galaxy

The derived lens model allows us to inspect the intrinsic properties of the un-lensed source from the observed images. In what follows, we only refer to the images I_1 and I_2 for which our lens model can accurately reproduce the observations. From the predicted magnifications, the magnitude of the un-lensed source is estimated as $i'_{AB} \approx 25.9$. This corresponds to a UV-luminosity of $F(1560\text{\AA}) = 6.3 \times 10^{40}$ erg/s/ \AA or $M(1560\text{\AA}) = -20.2$ mag. From this, we estimate a star formation rate (SFR) of the source galaxy to be $6M_{\odot}\text{yr}^{-1}$ without dust extinction correction (Madau et al. 1998). The observed Ly α flux indicates $\text{SFR} \sim 3M_{\odot}\text{yr}^{-1}$ (Kennicutt 1998; Brocklehurst 1971), which is lower than $\text{SFR}(1560\text{\AA})$. This is suggestive of dust extinction. Further, the superb HST/ACS angular resolution together with our lens model gives us size information of the source galaxy. The half-light radii r_h of the lensed images are listed in Table 1 (FLUX_RADIUS given by SExtractor: Bertin & Arnouts 1996). Note that even for the ACS images the FWHM of PSF is comparable to that of the lensed images. Taking this into account, we give a constraint on the intrinsic source size as $r_h \lesssim 0''.02$ ($r_{3\sigma} \lesssim 0''.08$; see Fig. 2), or $\lesssim 150$ pc ($\lesssim 600$ pc) in physical scales, assuming a simple one-dimensional amplification near the critical curve (see Ellis et al. 2001 for a similar case).

5. Summary

We report the discovery and spectroscopic confirmation of three gravitationally lensed images of a distant galaxy in the background of the rich cluster RXJ0152.7–1357 ($z = 0.83$). The similarity of the photometric and spectroscopic properties of the three images from Subaru observations provides strong evidence that they are gravitationally lensed images of a Ly α emitter at $z = 3.9$. A lens model was constructed on the basis of Jee et al.'s weak lensing mass estimates from the HST/ACS data. Our simple lens model can account simultaneously for the observed image configuration and the flux ratio of the closer

pair located close to the critical curve. The image parities in the ACS image are also consistent with the lensing hypothesis.

To further investigate the properties of this source galaxy at $z = 3.9$, we need longer wavelength data, such as K -band which samples its rest-frame B -band light or *Spitzer/Astro-F* bands at 3–8 μm which sample the light from underground old populations related to the stellar mass of this galaxy. A more detailed modeling of the lens mass distribution is important, as a well-constrained cluster mass model in conjunction with different sets of multiple images with suitable redshifts serves as a powerful probe of the geometry of the universe (Futamase & Yoshida 2001; Golse, Kneib, & Soucail 2002).

Acknowledgements

We acknowledge M. Chiba, M. Takada, T. Chiueh, and B.-C. Hsieh for useful discussions. We thank our referee, J.-P. Kneib, for his useful remarks helping to improve the paper. This work is financially supported in part by a Grant-in-Aid for the Scientific Research (No. 15740126) by the Ministry of Education, Culture, Sports, Science and Technology. M.T. acknowledges the JSPS research fellowship. Some of the data presented in this paper were obtained from the Multimission Archive at the Space Telescope Science Institute (MAST). STScI is operated by the Association of Universities for Research in Astronomy, Inc., under NASA contract NAS5-26555.

References

- Bartelmann, M., King, L.J., & Schneider, P., 2001, *A&A*, 378, 361
- Bertin, E. & Arnouts, S. 1996, *A&AS*, 117, 393
- Broadhurst, T. et al. 2005, *ApJ*, 621, 53
- Brocklehurst, M. 1971, *MNRAS*, 153, 471
- Chiba, M. 2002, *ApJ*, 565, 17
- Ellis, R. et al., 2001, *ApJ*, 560, L119
- Futamase, T & Yoshida, S. 2001, *Prog. Theor. Phys.*, 105, 887
- Golse, G., Kneib, J.-P., & Soucail, G. 2002, *A&A*, 387, 788
- Hattori, M., Kneib, J.-P., & Makino, N. 1999, *Prog. Theor. Phys. Suppl.*, 133, 1
- Hu, E.M. et al. 2002, *ApJ*, 568, L75
- Jee, M.J. et al. 2005, *ApJ*, 618, 46
- Kashikawa, N., et al. 2002, *PASJ*, 54, 819
- Kennicutt, R. C. 1998, *ARA&A*, 36, 189
- King, L.J. & Schneider, P. 2001, *A&A*, 369, 1
- Kneib, J.-P. et al., 1993, *A&A*, 273, 367
- Kneib, J.-P. et al., 1996, *ApJ*, 471, 643
- Kneib, J.-P. et al., 2003, *ApJ*, 598, 804
- Kneib, J.-P. et al., 2004, *ApJ*, 607, 697
- Kodama, T., et al. 2005, *PASJ*, 57, 309
- Kormann, R., Schneider, P., & Bartelmann, M. 1994, *A&A*, 286, 357
- Madau, P., Pozzetti, L., & Dickinson, M. 1998, *ApJ*, 498, 106
- Mellier, Y., Fort, B., & Kneib, J.-P., 1993, *ApJ*, 407, 33
- Molikawa, K. & Hattori, M., 1999, *ApJ*, 559, 544
- Pettini, M. et al., 2002, *ApJ*, 569, 742
- Schneider, P., Ehlers, J., & Falco, E.E. 1992, *Gravitational Lenses* (Springer-Verlag, Berlin)